Biomedicine & Pharmacotherapy 135 (2021) 111225

Contents lists available at ScienceDirect

Biomedicine & Pharmacotherapy

journal homepage: www.elsevier.com/locate/biopha

Original article

In-vivo wound healing activity of a novel composite sponge loaded with mucilage and lipoidal matter of *Hibiscus* species

Riham O. Bakr [a,*], Reham I. Amer [b,c], Dalia Attia [d], Mai M. Abdelhafez [e], Asmaa K. Al-Mokaddem [f], Abd El-Nasser G. El-Gendy [g], Ahlam M. El-Fishawy [h], Marwa A. A. Fayed [i], Sameh S. Gad [e]

[a] Department of Pharmacognosy, Faculty of Pharmacy, October University for Modern Sciences and Arts (MSA), 11787, Giza, Egypt
[b] Department of Pharmaceutics and Industrial Pharmacy, Faculty of Pharmacy, Al-Azhar University, Cairo, Egypt
[c] Department of Pharmaceutics, Faculty of Pharmacy, October University for Modern Sciences and Arts (MSA), Giza, Egypt
[d] Department of Pharmaceutics and Pharmaceutical Technology, Faculty of Pharmacy, The British University in Egypt (BUE), Cairo, Egypt
[e] Department of Pharmacology, Faculty of Pharmacy, October University for Modern Sciences and Arts (MSA), Giza, Egypt
[f] Department of Pathology, Faculty of Veterinary Medicine, Cairo University, 12211 Giza, Egypt
[g] Department of Medicinal and Aromatic Plants Research, National Research Center, Giza, 12622, Egypt
[h] Department of Pharmacognosy, Faculty of Pharmacy, Cairo University, 11562 Giza, Egypt
[i] Department of Pharmacognosy, Faculty of Pharmacy, University of Sadat City, 32897, Egypt

ARTICLE INFO

Keywords:
Hibiscus
Chitosan
Wound-healing sponge
Mucilage
Lipoidal matter

ABSTRACT

Many researches have been undergone to hasten the natural wound healing process. In this study, several *Hibiscus* species (leaves) were extracted with petroleum ether, methanol, and their mucilage was separated. All the tested species extracts were assessed for their viability percentage using the water-soluble tetrazolium. *H.syriacus* was the plant of choice to be incorporated in a new drug delivery system and evaluated for its wound healing activity. *H.syriacus* petroleum ether extract (PEE) showed a high percentage of palmitic and oleic acids while its mucilage demonstrated high glucosamine and galacturonic acid. It was selected to be formulated and pharmaceutically evaluated into three different composite sponges using chitosan in various ratios. Fourier-transformed infrared spectroscopy investigated the chemical interaction between the utilized sponges' ingredients. Morphological characteristics were evaluated using scanning electron microscopy. *H.syriacus* composite sponge of mucilage: chitosan (1:5) was loaded with three different concentrations of PEE. Medicated formulations were assessed in rat model of excision wound model. The wound healing ability was clearly proved by the clinical acceleration, histopathological examination, and modulation of correlated inflammatory parameters as tumor necrosis factor in addition to vascular endothelial growth factor suggesting a promising valuable candidate that supports the management of excision wounds using single-dose preparation.

1. Introduction

Wound healing is a complex process, which includes coordination between diverse immunological and biological systems. This involves many processes, inflammation, proliferation, accumulation of fibrous tissue, collagen deposition, contraction of the wound with the formation of granulation tissues, remodeling, and maturation [1]. Different herbal formulations have been reported to accelerate the process of wound healing by promoting epithelization, neovascularization, the formation of granulation tissue, collagen synthesis, wound contraction, tensile strength, etc [2]. Enhancing the normal wound healing process is considered one of the most important areas of research studies. Different new dressings and/or medicinal agents emerged to serve that important goal. With a cost approaching 25 billion $ in USA only in the past two decades; we can easily realize the importance of keep searching for a better solution and enrich the market with these lifesaving products [3,4]. Topical formulation represents an achievable and useful method that aids in the wound healing process [5]. Sponge technologies offer a suitable wound healing dressing especially in managing wounds with fluid exudates. The sponge which is considered as one of the widely used

* Corresponding author.
E-mail addresses: romar@msa.eun.eg, rehambkr@yahoo.com (R.O. Bakr).

https://doi.org/10.1016/j.biopha.2021.111225
Received 10 November 2020; Received in revised form 30 December 2020; Accepted 31 December 2020
Available online 1 February 2021

topical preparations could be defined as a dispersion of gas (usually air) into a solid matrix to give a porous solid structure [6]. A sponge dressing is formulated to grasp moisture on the surface of the wound and due to their high moisture content, they help to prevent bacteria and oxygen from reaching the wound providing a barrier that prevents infection. Additionally, it inhibits the loss of body fluids and accelerates the wound healing process [7].

Over three-quarters of the world population relies mainly on plants, plant extracts, or natural products for health care [8]. Concerning the wound healing remedy, more than 400 species of plants are identified as potentially useful alternative medicine [9]. Chitosan is a polysaccharide derived from naturally occurring chitin, that is considered as a commonly used biodegradable polymer in pharmaceutical preparations and an FDA approved food additive [10]. Chitosan displays unique polycationic, chelating, and film-forming properties due to the presence of active amino and hydroxyl functional groups. Chitosan also exhibits many interesting biological activities, including intrinsic antimicrobial activity, and its ability to deliver extrinsic antimicrobial agents to wounds and burns besides diverse stimulating or inhibiting activities toward several human cell types [11–13].

Family Malvaceae, (Mallow family), is well-known for its economic importance and wide folk medicinal uses, with 244 genera and 4225 species of plants distributed worldwide. *Hibiscus* is considered one of its biggest genera with 550 native species. *Hibiscus sabdariffa* L. (Roselle) has a diversity in its folk uses as being a hypotensive, diuretic, mild laxative, used in gastrointestinal ailments, antimicrobial, emollient, antipyretic, besides sedative effects [14]. Chemical characterization of *H.sabdariffa* showed the abundance of flavonoids as well as phenolic acids [15–18] justifying its folk use worldwide. Many biological activities have been demonstrated as an antioxidant [19], chemopreventive [20], cytotoxic and anti-inflammatory [21] anti-obesity [17], hypolipidemic [22], anti-anxiety, antidepressant [16], antihypertensive [23], as well as having a vasorelaxant effect [18].

Hibiscus syriacus L., an ornamental shrub, found throughout eastern and southern Asia, traditionally used as antifungal, febrifuge, in skin diseases, and as anthelmintic. Phytochemical study of roots showed the presence of triterpenoids [24,25], naphthalene, and lignans [26,27], coumarin [28], while leaves showed the presence of sterols and flavonoids [29], in addition to anthocyanidin malonyl glucosides in flowers [30]. Those bioactive compounds were contributors to different activities as an antidepressant and antidiabetic [24,25,27–29,31,32]

H.tiliaceous, is a shade tree conventionally used as antipyretic, cough sedative, and demulcent, relieving chest congestion, diarrhea, dysentery, and typhoid. Leaves and flowers were reported for their antioxidant, antibacterial antityrosinase, and analgesic activities [33,34], while flowers showed antidiabetic and hypolipidemic activities [35] correlated to the high phenolic contents [33]. Data about its phytochemistry is scarce, however, the main identified classes of phytoconstituents were friedelane-type triterpene, triterpenoids, coumarins, sterols, and amides [36,37].

H. rosa-sinensis, an ornamental shrub with leaves commonly used as a laxative [38]. The roots were used as cough sedatives, while the flowers have a diversity of uses as, aphrodisiac, emollient, and emmenagogue, besides the effect on fertility which was demonstrated by biological studies [39,40]. Biological effects such as antioxidant, anticonvulsant, hypoglycemic, antimicrobial [41–44], antiadipogenic [45], wound healing [46], inhibitory effect to melanoma [47] while its mucilage was tested as an excipient in tablet manufacture [48,49]. Reported phytoconstituents include flavonoids and phenolic acids contributing to anti-implantation activity [50], sterols, fatty acids, and pentacyclic triterpenoids [51].

In the pharmaceutical industry, there is an increased demand for biopolymers such as polysaccharides due to their ability to deliver unique physical functional characteristics [52]. Mucilage is a main class of phytoconstituents characterizing *Hibiscus* species, a hydrocolloid, which is hydrophilic in nature, used as a viscosity-enhancing agent, emulsifier, and gelling agent in topical preparation due to its ideal percutaneous absorption having a wide variety of therapeutic activities including wound healing, antidiabetic, antioxidant besides its binding and gelling properties, therefore a possible candidate for drug delivery modulation [53].

Oils derived from natural source have long been used on the skin for cosmetic and medical considerations. They may act as a protective barrier to the skin and retain moisture. Fatty acids have a role in immune and inflammatory responses. Essential fatty acids such as linoleic acid, ensure epidermal integrity while monounsaturated oleic acid increased skin permeability [54,55]. Sterols as well, such as tocopherol, a well-known antioxidant, and β-sitosterol, an angiogenic factor included in approved topical herbal preparation (MEBO ®)

In this study, several *Hibiscus* species were separately extracted with petroleum ether, methanol, and their mucilage was separated, their mineral content was compared and the viability potential of the different extracts was assessed. *H.syriacus* was further exposed to an in-depth phytochemical study, formulated in a sponge delivery system then further exposed to an excision wound model in rats.

2. Results and discussion

2.1. Determination of mineral content

Minerals have a great role as metalloenzymes, antioxidants besides being enzyme structural factors in healing wounds. In this study, and comparing the four studied species for their mineral content (Table 1), *H. syriacus* had the highest amount of Zn (10.54 mg) followed by *H. rosa-sinnesis*. Additionally, the highest Cu content was observed in *H. rosa-sinnesis* (6.42 mg) followed by *H. tiliaceus*, while *H. sabdariffa* showed the highest Se content this was followed by *H. syriacus* (0.25 mg) (Table 3). Zinc was reported to be essential for DNA replication in highly dividing cells as inflammatory and epithelial cells, and fibroblasts, in addition to its importance in collagen production, fibroblast proliferation, and epithelialization by stimulating the activity of involved enzymes [56]. Moreover, the importance of selenium as a powerful antioxidant and its ability to speed up wound healing has been reported [57].

2.2. Mucilage yield and characterization

Natural polysaccharides play an important role in the pharmaceutical industry as, an emulsifying agent, adhesive, thickener, viscosity enhancer, stability enhancer, and in pharmaceutical preparations [53]. Malvaceae is well known for its mucilage rich plants. Comparing the mucilage yield in the tested four species, the highest yield was obtained with *H.rosa-sinensis* (6 %), followed by *H.sabdariffa* (5 %), *H.syriacus* (4 %), and finally *H.tiliaceous* (3 %).

The swelling characteristics of *Hibiscus* species were highly different, where *H.syriacus* showed the highest swelling capacity (160 %), followed by *H.rosa-sinensis* (50 %), *H.tiliaceous* (30 %), while the lowest value was observed for *H.sabdariffa* (10.5 %). The higher swelling capacity estimated a higher water-holding capacity.

Analysis of monosaccharides in the *H.syriacus* mucilage (Table 2) showed the predominance of glucosamine 16.78 %, followed by galactose (2.17 %). Additionally, galacturonic acid (57.61 %) showed the highest concentration. The galacturonic acid and the high negative charge that it provides, besides the hydroxyl group, gives *H.syriacus* mucilage a high water holding capacity, increased surface area,

Table 1
Mineral composition (mg/kg).

Minerals	*H.sabdariffa*	*H.syriacus*	*H.rosa-sinensis*	*H.tiliaceous*
Cu	2.72	3.79	6.42	6.36
Zn	7.73	10.81	10.54	8.76
Se	0.32	0.25	0.23	0.12

Table 2
Composition of *H.syriacus* mucilage.

Carbohydrate	% of dry weight
Neutral sugar	
Glucosamine	16.78
Galactose	2.17
Uronic acid	
Galacturonic acid	57.61
Glucuronic acid	3.35
Glutric acid	6.65
Total identified	86.56 %

increased surface wettability, and water penetration giving higher hydrophilic nature providing an ability to maintain the skin water content besides being easily biodegradable [58–61]. Those results were in accordance with the previous report, where galacturonic acid was the main component [62].

2.3. Determination of H.sYriacus lipoidal content

GC–MS analysis of the unsaponifiable matter of *H.syriacus* (Table 3), revealed the presence of phytol (25.05 %), an unsaturated acyclic alcohol, a byproduct of chlorophyll degradation that was reported to stimulate the cell proliferation by enhancing its markers in human keratinocytes as well as ameliorating collagen production in dermal fibroblasts [63]. γ tocopherol (13.94 %) and β-sitosterol (9.24 %) were also reported for a potential wound healing effect both due to powerful antioxidant, as well as a plant angiogenic phytosterol successfully applied in chronic wound [64,65]. Additionally, palmitic acid was detected as the major saturated fatty acid (34.04 %), followed by linoleic acid (10.41 %) while the major unsaturated fatty acid was oleic acid (42.03 %) (Table 4). Palmitic acid was demonstrated to downregulate the pro-inflammatory cytokines (TNF-α and IL-12), besides a potential antimicrobial effect [66]. Furthermore, linoleic and oleic acids were proved to speed up the wound healing process by stimulating neutrophils to release vascular endothelial growth factor (VEGF-a), interleukin (IL-1b) and cytokine-induced neutrophil chemoattractant (CINC-2a/b) [54].

2.4. Proliferation assay

To evaluate and compare the cellular proliferation among all *Hibiscus* leaves extracts (petroleum ether, mucilage, and methanol) and choose

Table 3
GC–MS analysis of unsaponifiable matter of the *n*-hexane fraction of *H.syriacus*.

No.	RR_t (min)	Relative (%)	[M+] *m/z*	Component
1	0.5	2.06	206	5,5-Dimethyl-4-[3-Methyl-1,3-Butadienyl]-1-Oxaspiro[2.5]Octane
2	0.51	1.85	180	2(4 H)-Benzofuranone, 5,6,7,7a-tetrahydro-4,4,7a-trimethyl-, (R)
3	0.68	1.19	246	Benzene, (1-pentylheptyl)-
4	0.69	1.23	246	5-Phenyldodecane
5	0.74	2.26	246	1,3,3-Trimethylnonyl) benzene
6	0.76	1.69	290	13-phenylpentacosane
7	0.78	13.94	268	2-Pentadecanone, 61,014-trimethyl
8	0.82	1.77	310	Docosane
9	0.83	1.81	260	Benzene, (1-methyldodecyl)-
10	0.87	1.89	290	24,714-Tetramethyl-4-vinyl-tricyclo [5.4.3.0(1,8)] tetradecan-6-ol
11	0.98	3.67	450	Dotriacontane
12	1	25.05	296	Phytol
13	1.31	13.94	502	γ tocopherol
14	2.16	9.24	414	*β*-sitosterol
15	2.30	3.63	426	α-amyrin
16	2.41	4.49	426	*β*-amyrin
17	2.46	7.75	442	Betulin

Table 4
GC–MS analysis of fatty acids methyl esters of the *n*-hexane of *Hibiscus syriacus*.

No.	RR_t (min)	Relative %	Structure	[M+] *m/z*	Components
1	0.52	0.70	C9:0	216	Dimethyl azelate
2	0.68	1.95	C13:0	242	Methyl isomyristate
3	0.76	0.59	C14:0	256	Methylmyristate
4	0.85	34.04	C16:0	270	palmitic acid
5	0.90	0.62	C16:0	284	palmitic acid, ethyl ester
6	0.93	0.78	C17:0	284	margaric acid
7	0.99	10.41	C18:2	294	linoleic acid
8	1	42.03	C18:1	296	oleic acid
9	1.02	4.73	C18:0	298	Methyl isostearate
10	1.05	1.56	C17:0	310	Ethyl oleate
11	1.17	0.76	C20:0	326	arachidic acid
12	1.3	1.01	C22:0	354	Behenic acid
13	1.34	0.50	C23:0	368	Tricosanoic acid
Saturated fatty acids (%)					47.44
Unsaturated fatty acids (%)					52.4

the best representative, the water-soluble tetrazolium (WST-1) was used, as a rapid, simple, and sensitive method to measure cellular metabolic activity. *H.syriacus* petroleum ether extract and mucilage exposed to skin fibroblast at doses, 100 and 1000 µg/mL showed the highest viability and lowest toxicity with a percentage of viability ranging between 99.36 and 82.11 at the lowest concentration and 92.88 and 77.67 % at the highest concentration (Fig. 1). Therefore, due to the high safety margin of *H.syriacus*, and its high swelling capacity, it was chosen for pharmaceutical and pharmacological study.

2.5. Pharmaceutical formulation

The *H. syriacus* composite sponges were successfully formulated using different ratios of *H. syriacus* mucilage and chitosan (1: 1, 1: 3, and 1: 5) with the same amount of PEE of *H. syriacus*. The selection of the best formulation is based on the physical properties and the *in vitro* release of *β*-sitosterol from the prepared *H. syriacus* composite sponges (Table 5). The obtained *H. syriacus* composite sponges were dark brown, flexible with a porous structure, and of uniform weight, texture, and thickness. They have an elegant appearance with no visible cracks. Such combined properties increase the chance of these formulae to have a convenient application on the wound site.

2.5.1. Water uptake ability and Weight loss of prepared composite sponges

Water uptake capacity is one of the important parameters for biological claims for wound healing because it translates the sponge ability to absorb exudates from wounds besides providing a uniform release of the active constituent from sponges [67]. The water uptake of the observed sponges increased by increasing the ratio of chitosan to mucilage up to 5 (Table 6). This is principally due to the presence of amine and hydroxyl groups on the chitosan moiety, which is the most

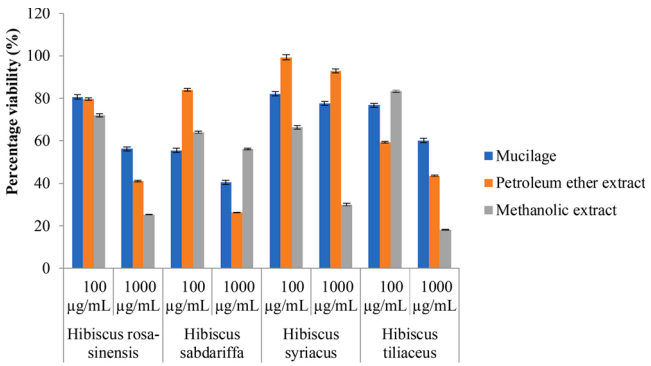

Fig. 1. Percentage of Viability of Different Extracts of Studied *Hibiscus* Species (n = 3, data are represented as mean ± SD).

Table 5
Composition of prepared *H. syriacus* composite sponges.

Mannitol[b] (%)	PEE of *H. syriacus*[a] µg/mL	Feeding ratio		Formula Code
		Chitosan	*H.syriacus* mucilage	
0.25	100	1	1	SPA
0.25	100	3	1	SPB
0.25	100	5	1	SPC

[a] Lyophilized powder of petroleum ether extract of *H. syriacus*.
[b] Mannitol used as a cryoprotectant.

Table 6
Physical parameter of the prepared sponges.

Weight loss (%) ± SD[a]	Water absorption (%) ± SD[a]	Formulae code
67 ± 8.74	270 ± 52.92	SPA
49 ± 10.5	310 ± 50.85	SPB
36.5 ± 7.29	543 ± 60.28	SPC

[a] Mean ± SD (n = 3).

likely site for the accommodation of the additional water due to its hydrophilicity [68]. Besides, the microporous structure within the sponges plays a significant role as it affects the water-retaining ability within the pores. The SPC offered maximum water uptake capacity among all the prepared sponge formulations; indeed the sponge can retain water in their porous structure surrounded by thick cell walls as the water uptake ability extends more than 500 %. Contrary, decreasing the amount of chitosan in the sponge led to smaller water uptake as the pores opening are surrounded by thin and friable walls. Also, the appearance of the fibrous networks in the sponge with lower chitosan content attenuates the ability of the water retained within pores [69]. Similar results were also reported in a previous study [70], which were subsequently confirmed by the weight loss of the sponges. This weight loss is in contrast with the increase in the chitosan ratio, as more chitosan can resist the dissolution in water.

2.5.2. Fourier transform infrared spectroscopy (FTIR)

FTIR was utilized to investigate any possible interactions between *H. syriacus* mucilage and chitosan at different blend ratios (Fig. 2). All the peaks in the IR spectrum of mucilage affirmed a polysaccharide structure. The characteristic peaks of chitosan were seen at 3428.81, 1631.4, and 1590 cm^{-1} corresponding to free alcoholic OH, amide and amino group, respectively. The FTIR spectrum of the *H.syriacus* mucilage showed a sharp and characteristic peak in the fingerprint region at 1040.4 cm^{-1} corresponding to C—O stretching vibration. The peak at 1627.6 cm^{-1} indicates the presence of aromatic C═C bending vibration. The sharp band at 2930.3 cm^{-1} is characteristic of methyl C—H stretching associated with the aromatic ring system. The characteristic absorption peak of $-NH_3^+$ shifted to 1622 cm^{-1} in the spectrums of the three formulated sponges with different intensity indicated the degree of ionic interaction between the negatively charged carboxylic ion group of *H.syriacus* mucilage and the positively charged amino group of chitosan in the three ratios of the blend [69,71].

2.5.3. Morphology of Composite Sponges: scanning electron microscopy (SEM)

Exploring the sponge morphology was essential to recognize the sponges' structure and well recognize their behavior. The morphological images of chitosan/ *H. syriacus* mucilage composite sponges is presented in Fig. 3, where, the sponges seemed as a highly porous structure while the coarseness of the sponge surface increased with rising the chitosan amount. Besides, the pore size decreased with increasing the chitosan content in the composite sponge. This was simply associated with the higher sponge density and is parallel to the effect of increased carrageenan content on the sponge structure previously reported [72].

2.5.4. Drug content

The loading of PEE (estimated as β-sitostetrol) in the sponges did not depart markedly from the calculated amount where > 95 % of active ingredient was recovered.

2.6. In-vitro release study

In-vitro release profile of chitosan/ *H. syriacus* mucilage composite sponges loaded with PEE was studied in phosphate buffer solution for 48 h. Although chitosan is a natural biodegradable polymer that gets solubilized at acidic pH, its solubility in basic pH is limited [73]. Therefore it was assured that all tested composite chitosan sponges remained intact in this buffer during the time of release assay. The average percentage release of β-sitosterol was nearly 95 %, 80 %, and 60 % for SPA, SPB, and SPC, respectively, in 48 h. It is worthy to say that the β-sitosterol release was markedly increased with a decrease of the chitosan amount in the prepared sponge (Fig. 4) as the polymer regains its gel structure upon sponge hydration with subsequent increase in diffusional path length of the drug which may interrupt the release profile. Moreover, thickening in the gel layer formed on the swollen sponge surface can prevent matrix disintegration and subside additional water penetration therefore delaying the drug release [74]. Besides increasing polymer content coupled with a smaller pore diameter as mentioned previously may obstruct the penetration of the solution into the matrices. By the end of release study, composite chitosan sponge is still intact

2.7. In-vivo wound healing activity

2.7.1. SPC induced rate of wound healing after 1 cm^2 excision wound induction

The rate of wound healing in male Wister rats treated once, on the wound induction day, with low to medium concentrations of *H. syriacus* sponge was significantly faster compared to both the control, non-treated group, (SPC-low, $p = 0.026$ and SPC-medium, $p = 0.037$) and the standard* treated group (SPC-low, $p = 0.031$ and SPC-medium, $p = 0.026$). Although the SPC-high didn't show a significant change compared to both the control or standard treated group, it showed a higher healing rate as shown in Fig. 5.

2.7.2. The inflammatory markers value restored in H. syriacus sponge treated wounds

At the end of the experiments, the inflammatory markers were measured in the healed skin using both immunohistochemistry and ELISA. Tissue expression of Tumor necrosis factor-α (TNF-α) in the wound area was demonstrated in Fig. 6A. All treated groups showed a significant decrease in TNF-α expression at the wound area compared to the non-treated control group. The latter was confirmed by the restoration of TNF-α values, in all treated groups, to the normal tissue value. The control group showed a significant increase regarding TNF-α release compared to normal skin tissue ($p = 0.0004$). There was a significant reduction in standard, SPC-plain, SPC-low, SPC-medium and SPC-high groups in compared to control group regarding TNF-α ($P < 0.0001, = 0.009$, 0.0009, 0.002 and < 0.0001 respectively as shown in Fig. 6A. The current study proved that SPC at low and medium doses not only enhances the wound healing process but also it modulates the main key players' cytokines. The good formation of stable newly generated healed tissue with proper collagen deposition and epithelial layer formation mainly depends on many cytokines and pathways [75]. The current study proved that the modulation of TNF-α levels greatly supports this theory by connecting the healing process with the modulation of such cytokines. SPC helps to restore the normal expression of TNF-α in the healed skin compared to the untreated wound. TNF-α is one of the most important parameters to assess the inflammation degree

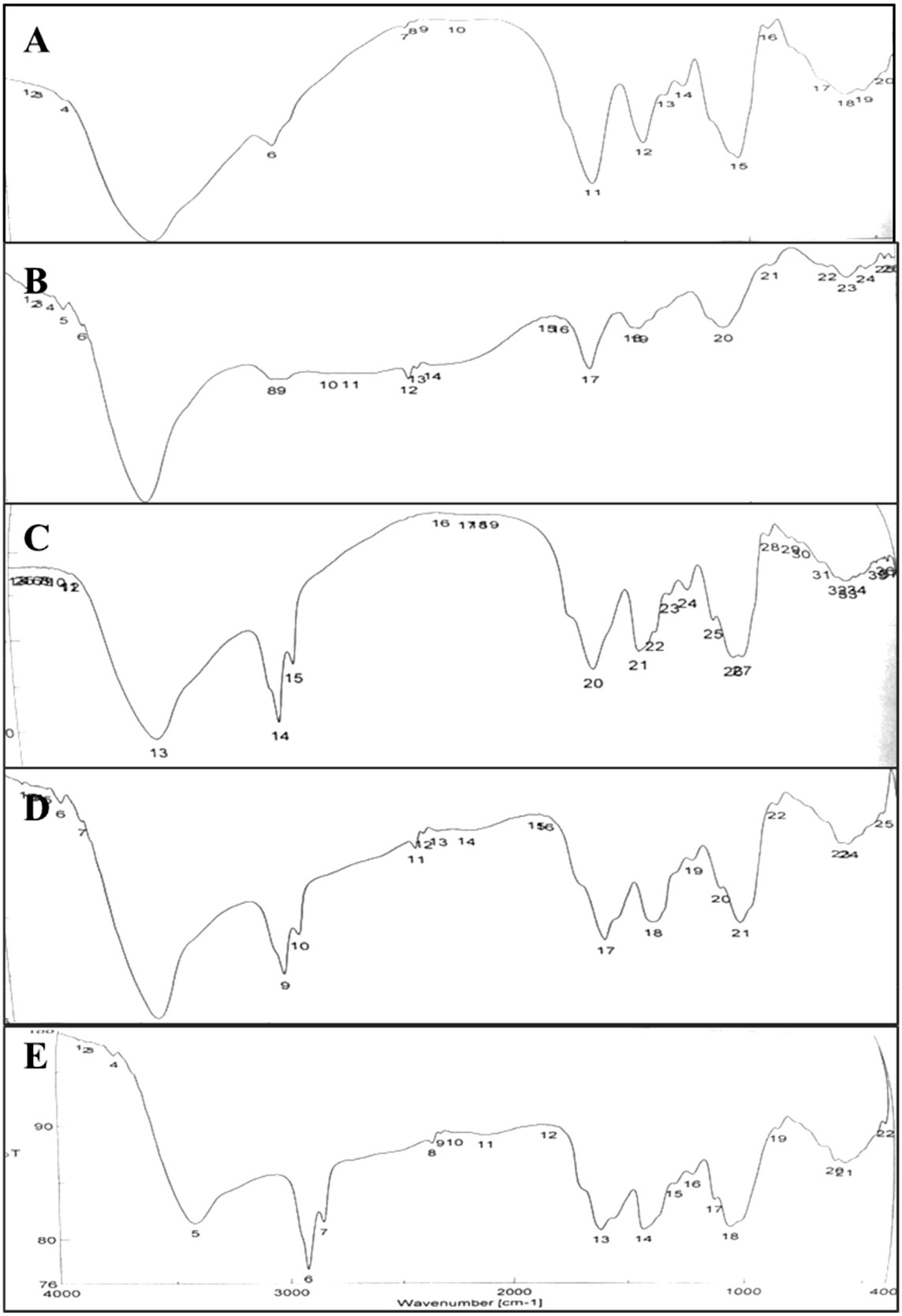

Fig. 2. FTIR spectra of **(a)** chitosan, **(b)** mucilage, **(c)** SPA, **(d)** SPB and **(e)** SPC.

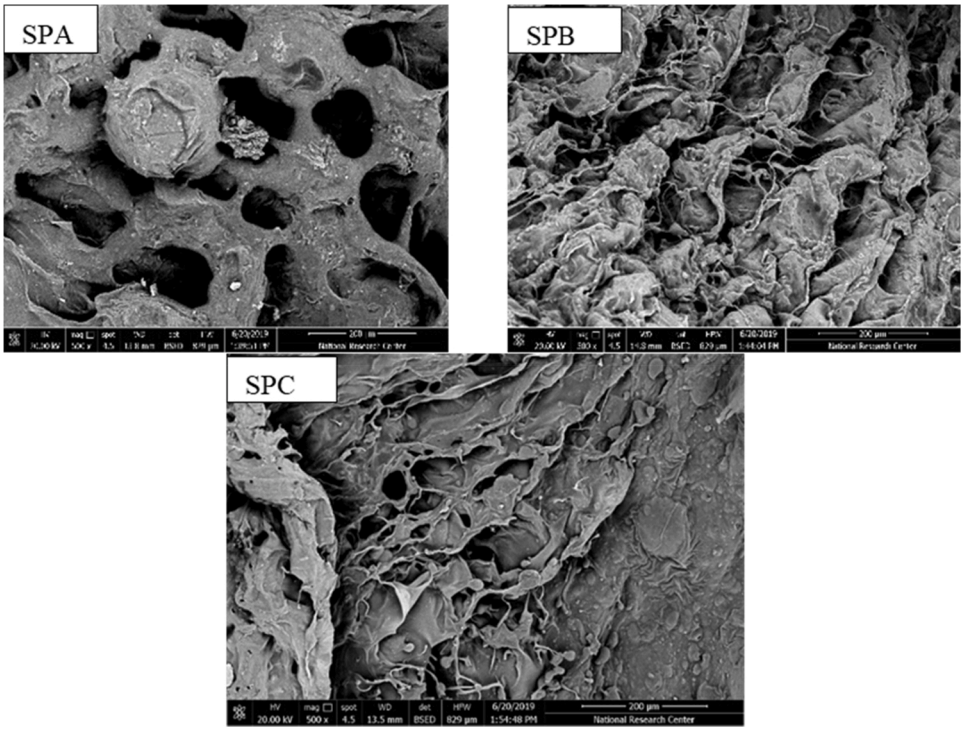

Fig. 3. SEM images of surface morphology of chitosan / *H. syriacus* mucilage composite sponges.

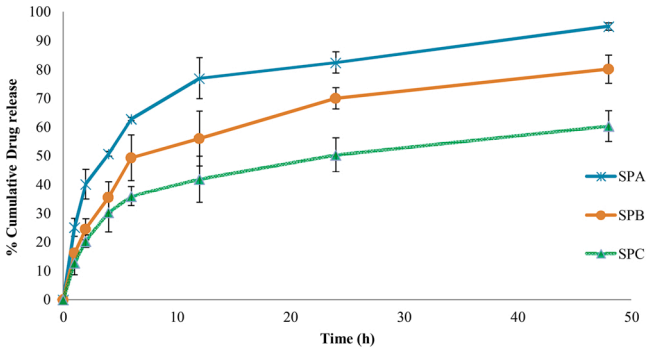

Fig. 4. The drug release behaviors of chitosan/ *H. syriacus* mucilage composite sponges loaded with *β*-sitosterol (n = 3, Mean ± SD).

during the healing process [76]. This is in line with a previous study [77] where the decrease in the TNF- α levels was associated with the fast wound repair mechanism upon the use of chamomile extract.

Transforming growth factor beta (TGF-β) in the healed tissue was significantly reduced in the control group compared to the normal non-wounded skin ($p = 0.004$), SPC-plain and SPC- low groups showed a similar effect. While there was a significantly increased value of standard and SPC-high treated groups compared to the control group ($p = 0.01$ and < 0.0001 respectively as shown in Fig. 6B. Regulation of both deposition and synthesis of extracellular matrix proteins such as osteonectin, fibronectin, collagen, and thrombospondin during the wound healing process solely depends on the active regulation of TGF-β. Also, degradation of the matrix is achieved via controlling levels of TGF-β which controls the expression of proteases such as MMP1, transin, collagenase, and plasminogen activator [78]. In a study showing the response to the usage of Korean Red ginseng, it demonstrated that in the early stages of wound healing there is an increased level of TGF-β [79]. However, in the present study, the levels of TGF-β after the wound healed didn't show differences with the untreated control except at a high concentration dose of SPC.

The gene expression of the vascular endothelial growth factor (VEGF) showed a significant increase in standard, SPC-plain, SPC-low, SPC-medium and SPC-high groups compared to control group ($P = 0.03$, <0.0001, < 0.0001, $= 0.0004$, and 0.02 respectively). The control group did not show any differences in comparison to the normal tissue as shown in Fig. 6C. VEGF represents the main pathway in angiogenesis, therefore, treatment with SPC upregulates the expression of VEGF which gives rise to the required new blood vessels essential for proper wound healing process [80]. This is in line with a previous study [79] where the use of Korean Red Ginseng increased significantly the VEGF levels of the wound healing process.

2.8. Histopathological examination

The examination of skin specimens from different experimental groups is illustrated in Fig. 7. Skin sections from the normal group showed normal histology of skin; the epidermis consisted of multiple layers of epithelial cells rested on an intact basement membrane and covered by the keratin layer. The dermis was formed of fibrous tissue containing skin-associated structures (adnexa) as hair follicles, sweat, and sebaceous glands. On contrary, the wounded area of skin in the control group exhibited serious histologic alterations; the epithelial cover was completely lost exposing the underlying tissue. The wound gap was filled with haphazardly arranged granulation tissue with inflammatory cell infiltrations. Numerous newly formed blood capillaries were observed at the base of the wound. Standard treated group showed retarded healing; the surface was covered completely by a thick serocellular crust composed of necrotic tissue debris and inflammatory exudates, beneath the crust only partial re-epithelization was noticed at the wound edges. The wound gap was filled by organized tissue with its characteristic perpendicular arrangement of the newly formed capillaries over the fibrous tissue. Intense inflammation was noticed. SPC-plain group exhibited better signs of healing, thickened hyperplastic epithelial cap was covering the wound area completely and the wound gap was filled by organized tissue with more collagen. Minimal inflammatory reaction was a prominent feature as well. The best healing criteria were observed in SPC-low group where the re-epithelization and

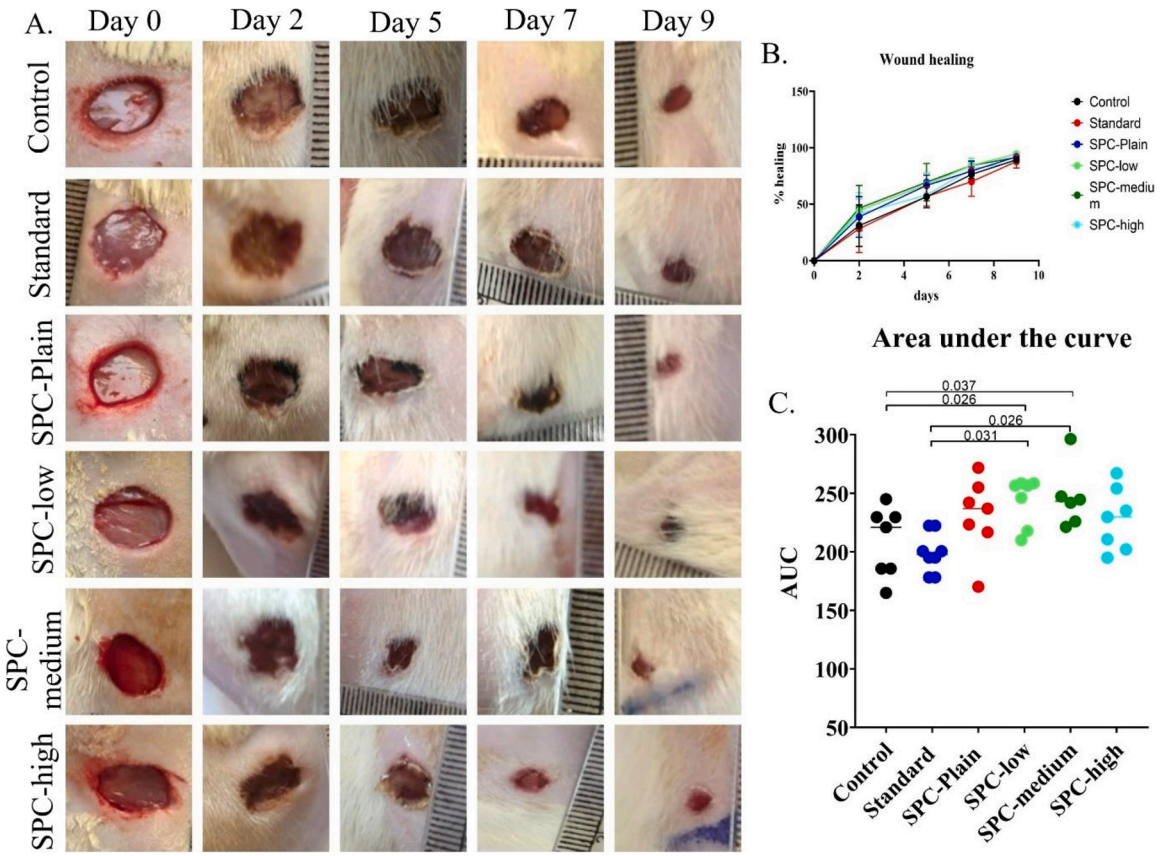

Fig. 5. Wound healing effect of different formulae concentration compared with standard marketed drug (Mebo®). The left panel (A) shows the rate of wound healing from day 0 (wound induction day) to day 9. The right panel (B) shows a quantitative measurement of area under the curve (AUC). Data are shown as scattered plot for each individual wound and represented as mean ± SD of at least 7 wounds. SPC- low and medium have $P < 0.05$ compared to control and standard, the exact P valve are shown in the graph.

epidermal remodeling were perfect; the wound surface was completely covered by regenerated epithelium with keratinization. The wound gap was filled by collagen-rich organized tissue. Few numbers of inflammatory cells were observed. In SPC-medium group, the wound was covered by a thick scab of inflammatory exudates and tissue debris. Beneath, a thin regenerated epithelial cover was observed, and the wound was filled by inflamed organized tissue. SPC-high group exhibited perfect epidermal remodeling and the wound area was containing collagen-rich organized tissue. Enhanced re-epithelization and perfect epithelial remodeling were observed in SPC treated groups compared to the control non-treated group. The standard group only exhibited mild improvement in epithelial healing. Generally, SPC- treated groups showed complete organization of the wound area with well-formed collagen fibers. Inflammatory cells infiltration was observed in all groups, but SPC-treated groups showed a numerical non-significant decrease in the intensity of the inflammatory reaction except SPC-low group that exhibited a significant decrease in inflammation score compared to the control group. Angiogenesis was improved significantly in both SPC-low and SPC-high groups. Standard and SPC-medium groups showed numerical improvement in the angiogenesis score. Concerning the collagen fibers evaluation (Fig. 8), MTC stained sections revealed a significant increase in collagen content at the wound area of all treated groups compared to the control group.

Re-epithelization is a pivotal histologic feature of ideal wound healing [81], perfect full-thickness re-epithelization with complete coverage of the wound area in all treated groups proves the ability of a single dose of SPC to promote and accelerate wound healing, and demonstrate the role of angiogenesis in wound healing as it is essential in providing the nutrients and oxygen supply required for wound repair [82]. SPC-treated groups showed an increase in capillaries formation compared to the non-treated groups that support their claimed role in tissue repair (Fig. 9). Collagen is one of the major components of extracellular matrix ECM related to the wound healing process and increasing the collagen content is a continuous process related to the progression of repair [83], the evidence of increased collagen in treated groups favor the positive impact of SPC on the process of wound closure.

3. Material and methods

3.1. Hibiscus species extraction

The leaves of *H.sabdariffa*, *H.syriacus*, *H.tiliaceous*, *H.rosa-sinensis* were collected in September 2018, from the Medicinal, Aromatic and poisonous Plants Experimental Station, Faculty of Pharmacy, Cairo University, Giza, Egypt. The plants were kindly identified by Dr. Mohammed El-Gebaly, senior botanist and consultant at Orman Botanical Garden. The voucher specimens (No.10–13/3/2019) were stored at the Herbarium of Faculty of Pharmacy, Cairo University.

The leaves (500 g) of each species were air- dried, defatted with petroleum ether using Soxhlet apparatus till exhaustion. The extracts were vacuum dried. The defatted plant material of each species was extracted with 70 % methanol, whereas the aqueous methanolic extracts were combined then vacuum dried. The dried residues of both petroleum ether and aqueous methanolic extracts were kept in refrigrerator at −20 °C prior to use for phytochemical and biological investigations.

3.2. Mucilage extraction

The cleaned, fresh leaves of the studied species were air-dried and ground. For yield estimation, 10 *g* of powdered leaves were macerated in

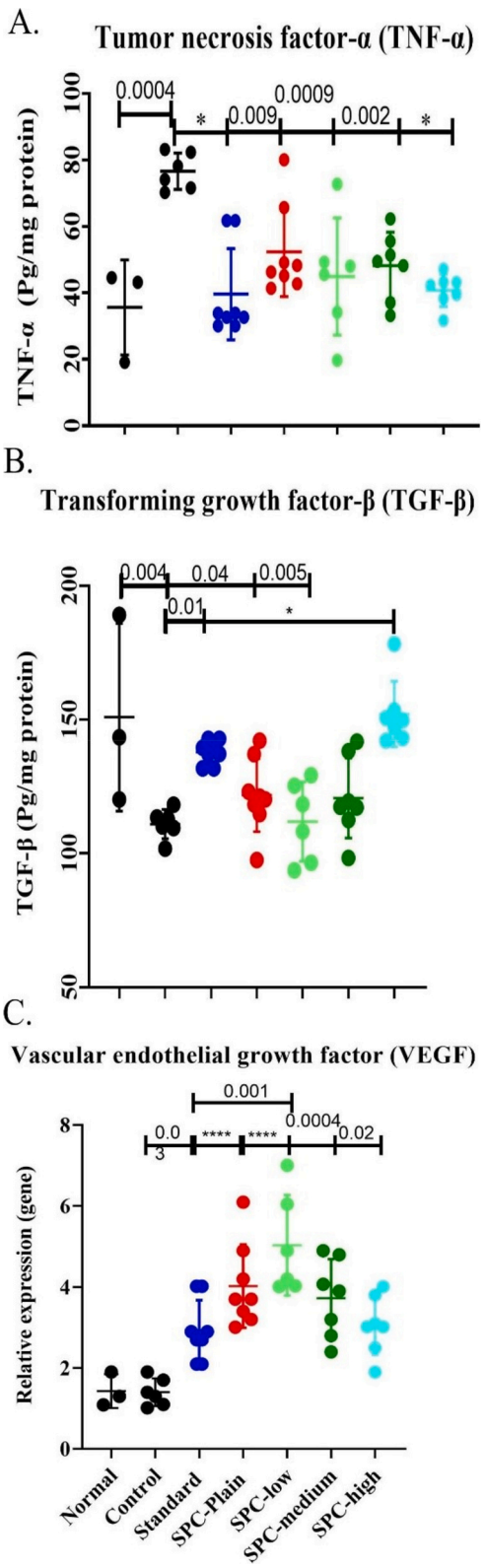

Fig. 6. Inflammatory and proliferative markers expression in the healed tissue. Quantitative analysis of the inflammatory markers in the healed tissue at the sacrifice day; tumor necrosis factor-α (A, TNF-α), transforming growth factor beta (B, TGF-β) and relative expression of vascular endothelial growth factor (C, VEGF). Data are shown as scattered plot for each individual wound and represented as mean ± SD of at least 7 wounds except normal skin n = 3. $P < 0.05$ compared to control group, * $P < 0.0001$, the exact P valve are shown in the graph.

water (80 mL), heated on a water bath at 50 °C for 5 h, the obtained slurry was centrifuged at 300 rpm (10 min.), the supernatant was mixed in the ratio 1:3 with 99 % ethanol, then centrifuged again at 3000 rpm for further 10 min. The obtained mucilage was then dried in a hot air oven at 60 °C overnight. The yield of the extracted mucilage was obtained by dividing the obtained dried mucilage weight by the weight of dried leaves used and expressed as % w/w yield [52]. The plant of choice (500 g) was further extracted using the same methodology keeping the same conditions.

3.3. Minerals estimation

Analysis of minerals in the *Hibiscus* leaves of the studied species was performed using atomic absorption spectroscopy. The leaves were weighed, heated in a quiet heater at 40 °C till there were no vapors, cooled at room temperature then moistened with concentrated H_2SO_4 and heated till fumes of H_2SO_4 ceased to evolve. The container with H_2SO_4 ash (one gram in 100 mL of 5 % HCl) was then heated for 2−3 h in a quiet heater at 60 °C till constant weight. The instrument measures the change in intensity which is converted into an absorbance related to the sample concentration [84].

3.4. Determination of swelling index

1.0 g of the dried mucilage was added in a graduated cylinder containing 100 mL of water, left for 24 h., and then the swollen volume was calculated as follows. $S = V_2 / V_1$; where S is the swelling index, V_2 is the volume of the mucilage prior to hydration, V_1 is the volume mucilage after hydration [85]

3.5. Monosaccharides and organic acids composition of Hibiscus mucilage

The mucilage of the chosen species having the highest viability percentage (cell proliferative assay) was subjected to HPLC analysis to identify and quantify the monosaccharides content and organic acids. 0.05 g of the mucilage was hydrolyzed using 4 M Trifluoro-acetic acid (10 mL), refluxed at 80 °C for 8 h., filtered through 0.45 μm, then injected into High-performance liquid chromatography-Refractive index detector (HPLC-RI) (Agilent1260, USA), The separation was achieved using isocratic elution using water with flow rate 0.6 mL/min. Peaks were identified based on their retention times, and quantified using, glucose, melezitose, galactose, mannose, fucose, fructose and one amino sugar (glucosamine) standards. Organic acids were separated by HPLC-UV (knauer, Germany), set at 214 nm, the flow rate was set at 0.6 mL/min, while the column oven temperature was kept constant at 65 °C, and the mobile phase was 0.005 M H_2SO_4 data. Integration was carried out by clarity-chrom software.

3.6. Determination of lipoidal matter

One gram of the petroleum ether extract of the chosen species (*H. syriacus*) with the highest viability percentage was refluxed with 5 % alcoholic KOH for 3 h., alcohol was distilled off, then the mixture was diluted with an equal volume of distilled water and the unsaponifiable matter (UNSAP) was extracted till exhaustion with extracted diethyl ether, which was combined, dried under reduced pressure, then kept for GC/MS analysis. The saponified *H.syriacus* extract was acidified with 5 N HCl, extracted thrice with diethyl ether, and then the combined extract was dissipated to dryness. The residue was methylated by refluxing for 3 h with 50:3 MeOH: H_2SO_4. The reaction mixture was extracted again thrice with diethyl ether where the combined extract was then dried and kept for GC/MS analysis for determination of fatty acid methyl ester (FAME) [86,87].

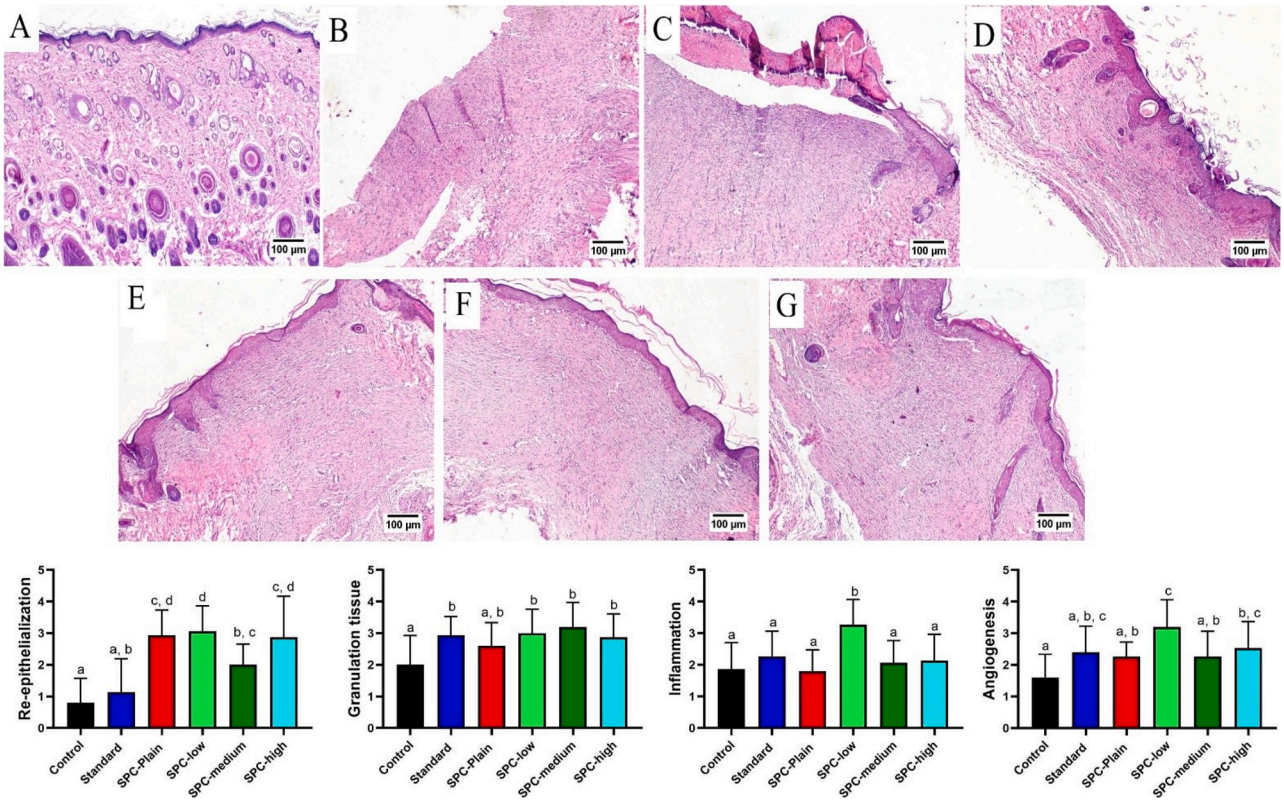

Fig. 7. Histopathological examination of the healed tissue. Photomicrograph of skin, H&E stained (A) Normal group, (B) Control, (C) Standard, (D) SPC-Plain, (E) SPC-low, (F) SPC-medium and (G) SPC-high. Charts, histopathological evaluation of re-epithelization, granulation tissue formation, inflammation, and angiogenesis. No histological alterations were detected in normal group. Data represented as mean ± SD of at least 4 wounds. a, b, c and d indicate significant difference at $P < 0.05$.

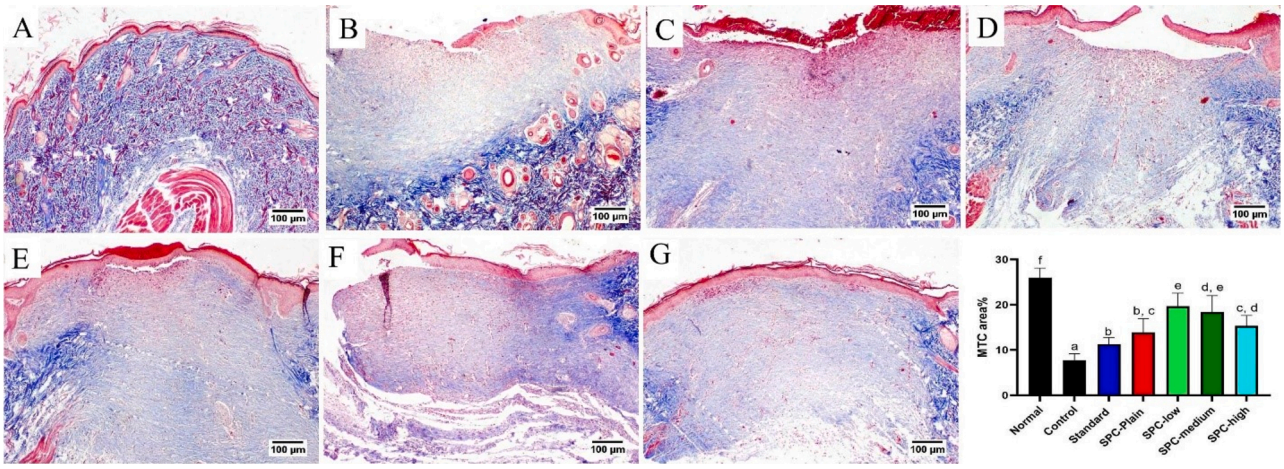

Fig. 8. Collagen formation in the healed tissue. Photomicrograph of skin, MTC stained (A) Normal group, (B) Control, (C) Standard, (D) SPC-Plain, (E) SPC-low, (F) SPC-medium and (G) SPC-high. Data represented as mean ± SD of at least 5 wounds except normal skin n = 3. a, b, c, d and e indicate significant difference at $P < 0.05$.

3.6.1. GC/MS analysis of UNSAP

UNSAP was analyzed on Shimadzu GCMS-QP2010 (Tokyo, Japan) where mass spectra were recorded. Rtx-5MS fused bonded column (30 m x0.25 mm i.d. × 0.25 µm film thickness) (Restek, USA) equipped with a split–splitless injector was used where the injector temperature was 280 °C while the initial column temperature was kept at 50 °C for 3 min (isothermal) that was programmed to 300 °C at a rate of 5 °C/min and kept constant at 300 °C for 10 min (isothermal) and Helium gas flow at 1.37 mL/min. Fragmentation was performed at 60 mA filament emission current, 70 eV ionization voltage 70 eV at 220 °C ion source. Confirmation of the hydrocarbons was achieved by comparison of their mass spectra with the NIST database and the available literature.

3.6.2. GC/MS analysis of FAME

FAME was analyzed using Shimadzu GCMS-QP2010 (Tokyo, Japan) equipped with Rtx-5 MS fused bonded column (30 m x0.25 mm i.d. × 0.25 µm film thickness) (Restek, USA) with a split–splitless injector. The initial column temperature was kept at 50 °C for 3 min (isothermal)

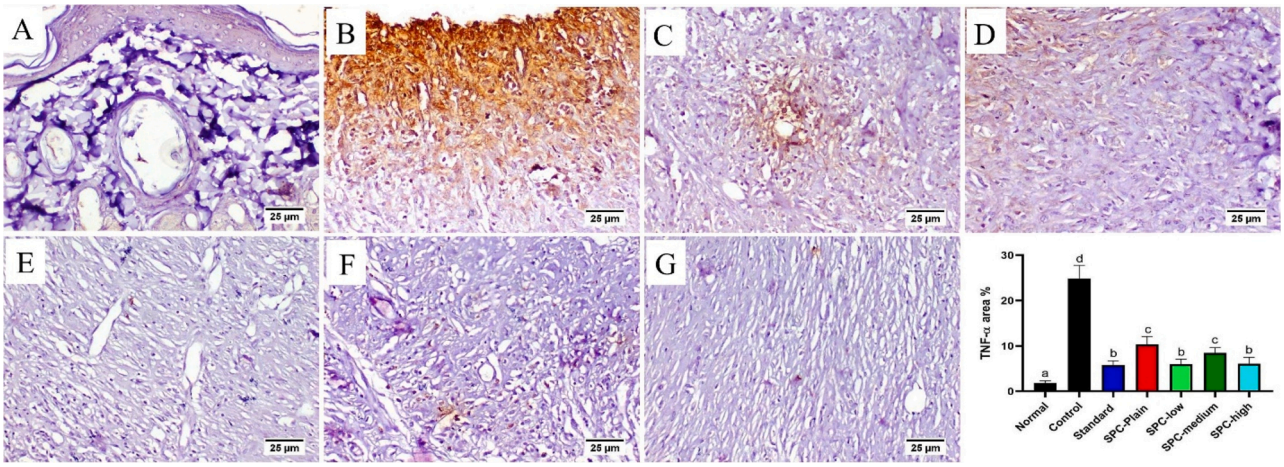

Fig. 9. Tumor necrosis factor- α expression on the healed tissue. Photomicrograph of skin, Immunostaining of TNF-α. (A) Normal group, (B) Control, (C) Standard, (D) SPC-Plain, (E) SPC-low, (F) SPC-medium and (G) SPC-high. Data represented as mean ± SD of at least 5 wounds except normal skin n = 3. a, b, c and d indicate significant difference at $P < 0.05$.

and programmed to 300 °C at a rate of 5 °C/min and kept constant at 300 °C for 10 min (isothermal), the injector temperature was 280 °C and the helium carrier gas flow rate was 1.37 mL/min. All the mass spectra were recorded following the usage of emission current, 60 mA; ionization voltage, 70 eV; ion source, 220 °C. Diluted samples (1% v/v) were injected with split mode (split ratio 1: 15). Matches for fatty acids were confirmed manually and by searching the NIST database using the NIST Mass Spectral Search Program.

3.7. Cell proliferative assay

Human skin fibroblast cell line was obtained by Nawah Scientific Inc., Cells were maintained in supplemented Dulbecco's modified eagle medium (DMEM) of streptomycin 100 mg/mL, Penicillin with 100 units/mL and heat-inactivated fetal bovine humidified serum with 10 %, carbon dioxide atmosphere 5 % (v/v) at 37 °C [88]. The proliferative assay was assessed by the Abcam® kit (ab155902 WST-1 Cell Proliferation Reagent. Human skin fibroblast cells (3×10^3 /well) were implanted in 96-well plates. After cell adhesion, different concentrations of plant leaves extracts (mucilage, petroleum ether, methanol; 100, 1000 µg/mL) were added, incubated for 48 h., then the proliferation was assessed using water-soluble tetrazoluim-1 (WST-1), and the absorbance was measured after an hour at $\lambda_{max.}$ 459 nm using a BMG LABTECH®-FLUOstar Omega microplate reader (Allmendgrün, Ortenberg) [89]. The assay was chosen as the criteria for further phytochemical, pharmaceutical and *in-vivo* study

3.8. Pharmaceutical formulation

3.8.1. Preparation of H. syriacus composite sponge

Chitosan solution (1% w/v) was prepared in 1% aqueous acetic acid at 25 °C. The slurry of *H. syriacus* mucilage was prepared by mixing the mucilage powder of *H. syriacus* (25 gm) in 100 mL water at room temperature then centrifuged to get rid of the precipitate. The composite mixtures were prepared by vigorously mixing the slurry of *H. syriacus* mucilage with a chitosan solution in different portions (1: 1, 1: 3, and 1: 5; *H. syriacus* mucilage: chitosan) using a magnetic stirrer (Wisestir1 (DAIHAN-Scientific Co., Ltd., Seoul, Korea) till obtaining homogenous consistency. 100 µg/mL of dried petroleum ether extract powder (PEE) of *H. syriacus* was added to the prepared homogenous mixture to form three formulae named; SPA, SPB, and SPC. The mixtures were then sonicated for five minutes to remove trapped air bubbles. Two ml of each homogenous mixture was poured into 8 wells of empty tablet strips with dimensions (2.5 × 2.5 cm2). The molded mixture subjected to freezing at −40 °C for 24 h preceding lyophilization step using lyophilizer (Lyph lock1 4.5, LABconco, Kansas, USA) at a vacuum set at 40 mTorr, for 10 h to obtain *H. syriacus* composite sponge.

3.8.2. Characterizations of H. syriacus composite sponge

3.8.2.1. Water uptake ability of H. syriacus composite sponge. The water absorption ability of *H. syriacus* composite sponge was measured through the incubation of known weight of composite sponge in phosphate-buffered saline (PBS) pH 7.4 at room temperature for 2 h, then the swollen sponge was weighted after being pressed gently between filter paper to ensure complete drying and remove the excess absorbed water on the surface, then weighed directly on an electronic balance scale.

The water content of the sponge was calculated as follows:

$$Ead = [W_e - W_0 / W_0] \times 100 \text{ [70]}$$

Where, Ead is the water absorption percentage of composite sponge at equilibrium, (W_e) is the weight of the mucilage-chitosan sponge at equilibrium, and (W_0) is the initial weight of the mucilage-chitosan sponge. The experiment was carried out in triplicate and data are offered as the mean of percentage water absorption ± SD (n = 3).

3.8.2.2. Weight loss of prepared composite sponges. The weight loss of the prepared composite sponges was carried out in triplicates. Samples of *H. syriacus* sponge were carefully merged in PBS solution pH 7.4 at 37 °C. After 24 h, the sponges were splashed with deionized water, frozen, lyophilized, and reweighing.

Weight loss of sponges was calculated as follows:

$$\% W = (W_0 - W_e) / W_0 \times 100 \text{ [70]}$$

Where (W_0) is the initial weight of sponge (g) and (W_e) is the weight lyophilized sponge (g).

3.8.2.3. Fourier-transformed infrared spectroscopy (FTIR). FTIR spectra of *H.syriacus* mucilage, chitosan, and *H.syriacus* mucilage: chitosan composite (with different ratios 1:1, 1:3, 1:5) were recorded using FTIR spectrophotometer equipped with deuterated triglycine sulfate (DTGS) detector and potassium bromide (KBr)/Germanium as a beam splitter. The instrument was connected to software OMNIC ver.9.7 and IR spectra were scanned at over the range of 650−4000 cm^{-1} and recorded for 32 scans at a resolution of 8 cm^{-1}. Each data point was recorded in three replicates using absorbance mode to facilitate quantitative analysis

[90].

3.8.2.4. Scanning electron microscopy (SEM). SEM (JSM 5300, JOEL, Japan) was used to detect the morphological structure of the prepared *H. syriacus* composite sponges, the sponge was placed on the sample holder of the SEM using adhesive strip in their both sides carefully not to damage the surface topography of the sponge, after that the sponge was covered with a thin layer of 150 A° gold and kept for two minutes in a 3×10^{-1} atm of argon (gas) in a vacuum and images picked up using i-scan 2000 software [91].

3.8.2.5. Drug content. Samples of *H.syriacus* sponges were weighed accurately and soaked in 50 mL of methanol, followed by sonication for 90 min. The methanolic solution was filtered using a 0.45 μm membrane filter and analyzed for *β*-sitosterol content using UV–vis spectrophotometry (Thermo Spectronic genesys 5, Haverhill, MA, USA) at λ_{208} nm. The actual content of *β*-sitosterol was estimated from the absorbance value, by comparison with the linear equation resulting using a serial dilution of *β*-sitosterol in pure methanol [92]. Each formulae was evaluated in triplicate and data are given as the mean ± SD (n = 3).

3.8.2.6. In-vitro drug release. Each composite sponge (2.5cm × 2.5cm) was immersed in glass vials with 20 mL phosphate buffer solution, pH 7.4 as releasing medium. The sealed vials were placed in a shaking water bath adjusted to 37 ± 0.5 °C and shaken at a regularity of 50 strokes/ min. All the supernatants were withdrawn periodically and swapped with an equivalent volume of fresh phosphate buffer solution. The samples were filtered by a 0.45 μm filter, and the amount of drug released was measured quantitatively using UV-spectrophotometry at a wavelength of λ_{208} nm [93]. *β*-sitosterol was chosen to represent the PEE. The concentration of released drug was then calculated using a standard curve of *β*-sitosterol in methanol. The percentage of *β*-sitosterol released was estimated as the following equation:

β-sitosterol release (%) = β-sitosterol released at time t / total β-sitosterol loaded in sponge × 100

All measurements were done in triplicates (mean ± SD).

Relying on the pharmaceutical evaluation results, the optimized *H. syriacus* composite sponge formulation was selected to be loaded with two other different concentrations of *H.syriacus* petroleum ether extract to investigate and compare their efficacy as medicated wound healing formulations (SPC-low, SPC-medium, and SPC-high) containing (100, 300, and 600 μg/mL *H.syriacus* PEE) respectively.

3.9. In-vivo determination of the wound healing activity

3.9.1. Animals

Twenty-four male Wister Albino rats (120−140 g) were obtained from VACSERA (The Egyptian Company for production of vaccines, sera and drugs). Animals were kept in MSA-animal house in plastic cages, with free access to food and water under standard room temperature while the light was maintained in a 12-h light and dark cycle. Animal experiments were in conformity with the MSA-ethical committee (Approval number PH6/EC6/2019). After 6 days of acclimatization, animals were randomly allocated into six groups (four animal/group), and two excision wounds were induced/ each animal. Sample size (n = 8) was calculated using G* Power 3.1.9 software, 80 % statistical power was used with alpha value = 0.05. The animal's groups were as follow, control group (saline), standard group (mebo®), plain group (SPC-plain) and 3 different treated groups with 3 different concentration of our tested material, assigned as (SPC-low, SPC-medium and SPC-high groups).

3.9.2. Excision wound

The experimental protocol has been previously described [94], briefly, the animals were anesthetized using intraperitoneal ketamine (70 mg/ kg) and xylazine (7 mg/kg). Dorsal hair was removed with depilatory cream, swabbed with 70 % alcohol for sterilization, then using a 1 cm biopsy punch, 2 wounds were made in the back of the rat, down to the fascia of the panniculus carnosus without breaking through it. Pictures of the wounds were taken before applying the treatment. Each group got one-time treatment on the day of wound induction. The animals were individually housed after the procedure, inspected daily for well-being, monitoring the wound and were pictured every other day for quantitatively measuring the rate of wound closure. Animal were sacrificed under ether anesthesia, skin samples from the healed wound were stored either, in formaldehyde at room temperature, for histopathology or in phosphate buffer saline at -20 °C for further biochemical markers.

3.9.3. Measurement of wound healing

Image J 1.52 software was used to measure the wound size quantitatively. A scaled picture from each wound was used to calculate the wound area in day 0, 2, 5, 7 and 9. Percentage of healing was measured using the following equation (100 – ((wound area at day n/wound area at day 0)*100)), where n = 2, 5, 7 or 9.

3.9.4. Wound healing markers

3.9.4.1. Enzyme-linked immunosorbent assay (ELISA). Transforming growth factor beta (TGF- β) (CSB-E04725 h) and Tumor necrosis factor-α (TNF-α) (MBS267654), were estimated using ELISA kit according to the manufacturer's instructions (Cusabio Life Sciences, Wuhan, China and MyBiosource, Inc., San Diego., USA respectively). Whereas, for TGF- β, tissue was rinsed with PBS to remove excess blood, chopped into 1−2 mm pieces, and homogenized with a tissue homogenizer in PBS or in lysate solution, lysate solution: tissue net weight = 10 mL : 1 *g* (i.e. Add 10 mL lysate solution to 1 g tissue), then centrifuged at approximately 5000 X g for 5 min, then assayed immediately or the homogenates were stored at -20 °C. Then the procedure and calculation were performed according to Rat TGF beta 1 ELISA Kit (Catalog Number MBS824788). For TNF-α, 100 mg tissue was rinsed with 1X PBS, homogenized in 1 mL of 1X PBS and stored overnight at -20 °C. After two freeze-thaw cycles were performed to break the cell membranes, the homogenates were centrifuged for 5 min. at 5000 x g, 2–8 °C. The supernatant was removed and assayed immediately. Alternatively, aliquots and stored samples at -20 °C or−80 °C. Centrifuge the sample again after thawing before the assay. Avoid repeated freeze-thaw cycles. Then the procedure and calculation were performed according to the Rat TNF-α ELISA Kit (Catalog Number.CSB-E11987 r).

3.9.4.2. Quantitative real time PCR (VEGF determination)

3.9.4.2.1. RNA extraction. Gene expression of VEGF were determined by Quantitative Real-Time polymerase chain reaction (qRT-PCR) in the tissue: 30 mg of tissue sample was excised and placed in vessel for disruption and homogenization. The tissue was disrupted, lysed in lysis Buffer RLT and the lysate was homogenized by tissue homogenizer for 40 s., followed by centrifugation for 3 min. at full speed, then the supernatant was carefully removed and transferred into a new microcentrifuge tube where 350 μl of 70 % ethanol was added to the cleared lysate. 700 μl of the sample, 500 μl Buffer RPE, 700 μl Buffer RW1 and 700 μl Buffer RW1 were transferred into spin column (RNeasy) and centrifuged for 30 s at 8000 rpm to allow effective washing of spin column membrane. Then placed in a new collection tube (1.5 mL) and 30−50 μl RNase free water was added and centrifuged for 1 min at 8000 rpm to elute the RNA. The supernatant was then transferred to a new Eppendorf tube to store at −80 °C for additional use. (A 260/ A280) purity obtained with the concentration of the RNA using spectrophotometry (dual wave length Beckman, spectrophotometer, USA).

3.9.4.2.2. cDNA synthesis. 3 μl of random primers were added to the

10 µl of RNA which was denatured for 5 min. at 65 °C in the thermal cycler. The RNA primer mixture was cooled to 4 °C and the cDNA master mix was prepared (19 µl) according to the kit instructions then added to 31 µl RNA-primer mixture which result in 50 µl cDNA. The mixture was incubated in the preprogrammed thermal cycler for one hour (37 °C) then inactivation of enzymes (90 °C) for 10 min. and at last cooled at (4 °C), RNA was changed to cDNA which stored at (20 °C).

3.9.4.2.3. Real-time qPCR using SYBR green I. Real-time qPCR amplification and analysis were performed using an Applied Biosystem with software version 3.1 (StepOne™, USA). The qPCR assay with the primer sets were optimized at the annealing temperature.

3.9.4.2.4. Primers used (VEGF determination). Forward primer : 5′-ATCATGCGGATCAAACCTCACC3′

Reverse primer:5′- GGTCTGCATTCACATCTGCTAT3′

β-actin

Forward primer :5′-CAG GAT GGC GTG AGG GAG AGC-3′

Reverse primer: 5′-AAG GTG TGA TGG TGG GAA TGG-3′

3.9.4.2.5. Calculation of relative quantification (RQ) (relative expression). The relative quantitation was calculated according to Applied Bio system software using the following equation

$$\Delta \text{ Ct} = \text{Ct gene test} - \text{Ct endogenous control}$$

$$\Delta\Delta\text{Ct} = \Delta\text{Ct sample1} - \Delta\text{Ct calibrator}$$

$$\text{RQ} = \text{Relative quantification} = 2\text{-}\Delta\Delta\text{Ct}$$

The RQ is the fold change compared to the calibrator (untreated sample)

3.10. Histopathological examination

Tissue specimen from the skin wound were fixed in 10 % neutral formalin saline, routinely processed by passage in grades of alcohols and xylene, embedded in paraffin wax and stained with hematoxylin and eosin (H&E) and Masons trichrome stain (MTC) [95]. Tissue slides were examined under light microscope, Olympus BX43 connected to Olympus DP-27 digital camera. Histologic scoring was done according to previous report [96], briefly a score ranging from 0 to 4 was given to the degree of re-epithelialization (0=Absence of epithelial proliferation, 1=Poor epidermal organization, 2= Incomplete epidermal organization, 3=Moderate epithelial proliferation and 4= Complete epidermal remodeling), granulation tissue and collagen matrix organization (0=Immature granulation and inflammatory tissue, 1=Thin immature and inflammatory tissue, 2= Moderate remodeling, 3=Thick granulation layer and well-formed collagen and 4=Complete organized tissue), degree of inflammation (0 = 13–15 inflammatory cells per histological field, 1 = 10–13 inflammatory cells per histological field, 2 = 7–10 inflammatory cells per histological field, 3 = 4–7 inflammatory cells per histological field and 4 = 1–4 inflammatory cells per histological field) and angiogenesis (0= Absence of angiogenesis and presence of congestion, hemorrhage, edema, 1 = 1−2 vessels per site with edema, hemorrhage, congestion, 2 = 3–4 vessels per site, moderate edema, congestion, 3 = 5–6 vessels per site, slight edema, congestion, 4=More than 7 vessels per site vertically disposed toward the epithelial surface). MTC stained sections were used to demonstrate collagen fibers. MTC stained areas were quantified as (area %) using Cellsens dimensions (Olympus software).

3.11. Immunohistochemistry

Prepared paraffin blocks were used to cut 5 µm sections on positively charged slides for immunostaining. After deparaffinization and rehydration, tissue sections were subjected to heat-induced epitope retrieval in microwave followed by blocking against endogenous peroxidases. Tissue sections were washed in PBS and incubated with monoclonal mouse anti- TNF-α antibodies (Santa Cruz Biotechnology, Inc.) overnight in refrigerator. After washing, HRP-labelled secondary antibody (Abcam, UK) was applied for 2 h at room temperature. DAB-substrate detection kit (Thermofisher, USA) was used to visualize the reaction. Negative control slides were obtained by removal of primary antibody. Positive staining was quantified and expressed as area % using CellSens dimensions (Olympus software).

4. Conclusion

This study demonstrated the promising and potential wound healing effect of *H.syriacus* loaded in a novel composite sponge formulated with bioactive polysaccharides (chitosan and leaf mucilage) besides the petroleum ether extract and evaluated in an *in-vivo* rat model. *H.syriacus* showed the presence of minerals, fatty acids, and sterols that demonstrated good correlation with the wound healing effect. Topical application of single dose of the formulated sponge resulted in accelerating wound closure through a potential decrease in TNF-α, and increase in both TGF-β and VEGF resulting in enhanced re-epithelization, angiogenesis and perfect epithelial remodeling.

Funding

This research did not receive any specific grant from funding agencies in the public, commercial, or not-for-profit sectors.

CRediT authorship contribution statement

Riham O. Bakr: Conceptualization, Methodology, Investigation, Data curation, Writing - review & editing. **Reham I. Amer:** Conceptualization, Methodology, Investigation, Data curation. **Dalia Attia:** Methodology, Investigation, Data curation. **Mai M. Abdelhafez:** Investigation, Formal analysis, Data curation. **Asmaa K. Al-Mokaddem:** Investigation, Formal analysis, Data curation. **Abd El-Nasser G. El-Gendy:** Data curation. **Ahlam M. El-Fishawy:** Supervision. **Marwa A. A. Fayed:** Data curation, Writing - review & editing. **Sameh S. Gad:** Investigation, Formal analysis, Data curation.

Declaration of Competing Interest

The authors declare no conflict of interest.

References

[1] A. Bhaskar Rao, E. Prasad, S.S. Deepthi, V. Haritha, S. Ramakrishna, K. Madhusudan, M.V. Surekha, Y.S.R. Venkata Rao, Wound healing: a new perspective on glucosylated tetrahydrocurcumin, Drug Des. Devel. Ther. 9 (2015) 3579–3588, https://doi.org/10.2147/DDDT.S85041.

[2] B. Nagoba, M. Davane, Studies on wound healing potential of topical herbal formulations- do we need to strengthen study protocol? J. Ayurveda Integr. Med. 10 (2019) 316–318, https://doi.org/10.1016/j.jaim.2019.09.002.

[3] C.K. Sen, G.M. Gordillo, S. Roy, R. Kirsner, L. Lambert, T.K. Hunt, F. Gottrup, G. C. Gurtner, M.T. Longaker, Human skin wounds: a major and snowballing threat to public health and the economy: PERSPECTIVE ARTICLE, Wound Repair Regen. 17 (2009) 763–771, https://doi.org/10.1111/j.1524-475X.2009.00543.x.

[4] Z. Bagher, A. Ehterami, M.H. Safdel, H. Khastar, H. Semiari, A. Asefnejad, S. M. Davachi, M. Mirzaii, M. Salehi, Wound healing with alginate/chitosan hydrogel containing hesperidin in rat model, J. Drug Deliv. Sci. Technol. 55 (2020) 101379, https://doi.org/10.1016/j.jddst.2019.101379.

[5] D. Gopinath, M.R. Ahmed, K. Gomathi, K. Chitra, P.K. Sehgal, R. Jayakumar, Dermal wound healing processes with curcumin incorporated collagen films, Biomaterials 25 (2004) 1911–1917, https://doi.org/10.1016/S0142-9612(03)00625-2.

[6] H.L. Lai, A. Abu'Khalil, D.Q.M. Craig, The preparation and characterisation of drug-loaded alginate and chitosan sponges, Int. J. Pharm. 257 (2003) 175–181, https://doi.org/10.1016/S0378-5173(02)00590-2.

[7] J. Dutta, Synthesis and characterization of γ-irradiated PVA/PEG/CaCl2 hydrogel for wound dressing, Am. J. Chem. 2 (2012) 6–11, https://doi.org/10.5923/j.chemistry.20120202.02.

[8] S. Yogisha, K. Raveesha, In-vitro antibacterial effect of selected medicinal plant extracts, J. Nat. Prod. 2 (2009) 64–69.

[9] P.K. Ghosh, A. Gaba, Phyto-extracts in wound healing, J. Pharm. Pharm. Sci. 16 (2013) 760–820, https://doi.org/10.18433/j3831v.

[10] H. Ueno, T. Mori, T. Fujinaga, Topical formulations and wound healing applications of chitosan, Adv. Drug Deliv. Rev. 52 (2001) 105–115, https://doi.org/10.1016/S0169-409X(01)00189-2.

[11] B. Wang, K. Chen, S. Jiang, F. Reincke, W. Tong, D. Wang, C. Gao, Chitosan-mediated synthesis of gold nanoparticles on patterned poly(dimethylsiloxane) surfaces, Biomacromolecules 7 (2006) 1203–1209, https://doi.org/10.1021/bm060030f.

[12] H. Yi, L.Q. Wu, W.E. Bentley, R. Ghodssi, G.W. Rubloff, J.N. Culver, G.F. Payne, Biofabrication with chitosan, Biomacromolecules 6 (2005) 2881–2894, https://doi.org/10.1021/bm050410l.

[13] T. Dai, M. Tanaka, Y.Y. Huang, M.R. Hamblin, Chitosan preparations for wounds and burns: antimicrobial and wound-healing effects, Expert Rev. Anti. Ther. 9 (2011) 857–879, https://doi.org/10.1586/eri.11.59.

[14] H.D. Neuwinger, African Traditional Medicine. A Dictionary of Plant Use and Application, Medpharm Scientific: Stuttgart, Germany, 2000.

[15] I. Da-Costa-Rocha, B. Bonnlaender, H. Sievers, I. Pischel, M. Heinrich, Hibiscus sabdariffa L. - A phytochemical and pharmacological review, Food Chem. 165 (2014) 424–443, https://doi.org/10.1016/j.foodchem.2014.05.002.

[16] A. Gulsheen, A. Kumar, Sharma, Antianxiety and antidepressant activity guided isolation and characterization of Gossypetin from Hibiscus sabdariffa linn, Calyces, J. Biol. Act. Prod. from Nat. 9 (2019) 205–214, https://doi.org/10.1080/22311866.2019.1615552.

[17] O.V. Ojulari, S.G. Lee, J.O. Nam, Beneficial effects of natural bioactive compounds from Hibiscus sabdariffa L. On obesity, Molecules 24 (2019) 210–224, https://doi.org/10.3390/molecules24010210.

[18] A.M. Zheoat, A.I. Gray, J.O. Igoli, V.A. Ferro, R.M. Drummond, Hibiscus acid from Hibiscus sabdariffa (Malvaceae) has a vasorelaxant effect on the rat aorta, Fitoterapia 134 (2019) 5–13, https://doi.org/10.1016/j.fitote.2019.01.012.

[19] P. Subhaswaraj, M. Sowmya, V. Bhavana, M. Dyavaiah, B. Siddhardha, Determination of antioxidant activity of Hibiscus sabdariffa and Croton caudatus in Saccharomyces cerevisiae model system, J. Food Sci. Technol. 54 (2017) 2728–2736, https://doi.org/10.1007/s13197-017-2709-2.

[20] A.C.G.V. Gheller, J. Kerkhoff, G.M. Vieira Júnior, K.E. De Campos, M.M. Sugui, Antimutagenic effect of Hibiscus sabdariffa L. Aqueous extract on rats treated with monosodium glutamate, Transfus. Apher. Sci. 2017 (2017) 8, https://doi.org/10.1155/2017/9392532. Article ID 9392532.

[21] P. Worawattananutai, A. Itharat, S. Ruangnoo, In vitro antioxidant, anti-inflammatory, cytotoxic activities against prostate cancer of extracts from Hibiscus sabdariffa leaves, J. Med. Assoc. Thai. 97 (2014) S81–87.

[22] S. Gosain, R. Ircchiaya, P.C. Sharma, S. Thareja, A. Kalra, A. Deep, T.R. Bhardwaj, Hypolipidemic effect of ethanolic extract from the leaves of Hibiscus sabdariffa L. In hyperlipidemic rats, Acta Pol. Pharm. - Drug Res. 67 (2010) 179–184.

[23] S.A. Nurfaradilla, F.C. Saputri, Y. Harahap, Effects of Hibiscus sabdariffa calyces aqueous extract on the antihypertensive potency of Captopril in the two-Kidney-one-clip rat hypertension model, Evidence-Based Complement, Altern. Med. 2019 (2019) 7, https://doi.org/10.1155/2019/9694212. Article ID 9694212.

[24] R.J. Hsu, Y.C. Hsu, S.P. Chen, C.L. Fu, J.C. Yu, F.W. Chang, Y.H. Chen, J.M. Liu, J. Y. Ho, C.P. Yu, The triterpenoids of hibiscus syriacus induce apoptosis and inhibit cell migration in breast cancer cells, BMC Complement. Altern. Med. 15 (2015) 65–74, https://doi.org/10.1186/s12906-015-0592-9.

[25] L.S. Shi, C.H. Wu, T.C. Yang, C.W. Yao, H.C. Lin, W.L. Chang, Cytotoxic effect of triterpenoids from the root bark of Hibiscus syriacus, Fitoterapia 97 (2014) 184–191, https://doi.org/10.1016/j.fitote.2014.05.006.

[26] S.W. Yeon, H.Y. Kwon, J.I. Nam, J.H. Ahn, Y.H. Jo, A. Turk, Y.J. Lee, D.H. Shin, B. Y. Hwang, M.K. Lee, Three new naphthalenes from the roots of Hibiscus syriacus, Phytochem. Lett. 33 (2019) 110–113, https://doi.org/10.1016/j.phytol.2019.08.012.

[27] S.J. Lee, Y.S. Yun, I.K. Lee, I.J. Ryoo, B.S. Yun, I.D. Yoo, An antioxidant lignan and other constituents from the root bark of Hibiscus syriacus, Planta Med. (1999), https://doi.org/10.1055/s-2006-960841.

[28] B.S. Yun, I.K. Lee, I.J. Ryoo, I.D. Yoo, Coumarins with monoamine oxidase inhibitory activity and antioxidative coumarino-lignans from Hibiscus syriacus, J. Nat. Prod. 64 (2001) 1238–1240, https://doi.org/10.1021/np0100946.

[29] Q. Wei, X. ying Ji, F. Xu, Q. rong Li, H. Yin, Chemical constituents from leaves of Hibiscus syriacus and their α-Glucosidase inhibitory activities, Zhong Yao Cai 38 (2015) 975–979.

[30] J.H. Kim, G.I. Nonaka, K. Fujieda, S. Uemoto, Anthocyanidin malonylglucosides in flowers of Hibiscus syriacus, Phytochemistry 28 (1989) 1503–1506, https://doi.org/10.1016/S00319422(00)97774-4.

[31] Y.L. Cheng, S.C. Lee, H.J. Harn, H.C. Huang, W.L. Chang, The extract of Hibiscus syriacus inducing apoptosis by activating p53 and AIF in human lung cancer cells, Am. J. Chin. Med. 36 (2008) 171–184, https://doi.org/10.1142/S0192415X08005680.

[32] Y.H. Kim, A.R. Im, B.K. Park, S.H. Paek, G. Choi, Y.R. Kim, W.K. Whang, K.H. Lee, S.E. Oh, M.Y. Lee, Antidepressant-like and neuroprotective effects of ethanol extract from the root bark of Hibiscus syriacus L, Biomed Res. Int. (2018), https://doi.org/10.1155/2018/7383869.

[33] S.K. Wong, Y.Y. Lim, E.W.C. Chan, Evaluation of antioxidant, anti-tyrosinase and antibacterrial activities of selected Hibiscus species, Ethobotanical Leafl. 14 (2010) 781–796.

[34] F. Qiu, H. Tian, Z. Zhang, X.L. Yuan, Y.F. Tan, X.Q. Ning, Pharmacological study on hemostasis, analgesic and anti inflammation effects of the alcohol extract of Hibiscus tiliaceus, Zhong Yao Cai 36 (2013) 1648–1651.

[35] S. Kumar, V. Kumar, O. Prakash, Antidiabetic and hypolipidemic activities of hibiscus tiliaceus (L.) flowers extract in streptozotocin induced diabetic rats, Pharmacologyonline 2 (2010) 1037–1044.

[36] L. Li, X. Huang, I. Sattler, H. Fu, S. Grabley, W. Lin, Structure elucidation of a new friedelane triterpene from the mangrove plant Hibiscus tiliaceus, Magn. Reson. Chem. 44 (2006) 624–628, https://doi.org/10.1002/mrc.1802.

[37] J.J. Chen, S.Y. Huang, C.Y. Duh, I.S. Chen, T.C. Wang, H.Y. Fang, A new cytotoxic amide from the stem wood of Hibiscus tiliaceus, Planta Med. 72 (2006) 935–938, https://doi.org/10.1055/s-2006-931604.

[38] A.H. Gilani, S. Bashir, K.H. Janbaz, A.J. Shah, Presence of cholinergic and calcium channel blocking activities explains the traditional use of Hibiscus rosasinensis in constipation and diarrhoea, J. Ethnopharmacol. 102 (2005) 289–294, https://doi.org/10.1016/j.jep.2005.07.023.

[39] N. Vasudeva, S.K. Sharma, Post-coital antifertility activity of Hibiscus rosa-sinensis Linn. roots, evidence-based complement, Altern. Med. 5 (2008) 91–94, https://doi.org/10.1093/ecam/nem003.

[40] S.D. Kholkute, Effect of Hibiscus rosa sinensis on spermatogenesis and accessory reproductive organs in rats, Planta Med. 31 (1977) 92–127, https://doi.org/10.1055/s-0028-1097504.

[41] D. Garg, A. Shaikh, A. Muley, T. Marar, In-vitro antioxidant activity and phytochemical analysis in extracts of Hibiscus rosa-sinensis stem and leaves, Free. Radic. Antioxid. 2 (2012) 41–46, https://doi.org/10.5530/ax.2012.3.6.

[42] V.S. Kasture, C.T. Chopde, V.K. Deshmukh, Anticonvulsive activity of Albizzia lebbeck, Hibiscus rosa sinesis and Butea monosperma in experimental animals, J. Ethnopharmacol. 71 (2000) 65–75, https://doi.org/10.1016/S0378-8741(99)00192-0.

[43] A. Sachdewa, R. Nigam, L.D. Khemani, Hypoglycemic effect of Hibiscus rosa sinensis L. Leaf extract in glucose and streptozotocin induced hyperglycemic rats, Indian J. Exp. Biol. 39 (2001) 284–286.

[44] S. Vijayakumar, J.E. Morvin Yabesh, P. Arulmozhi, P.K. Praseetha, Identification and isolation of antimicrobial compounds from the flower extract of Hibiscus rosa-sinensis L: in silico and in vitro approaches, Microb. Pathog. 123 (2018) 527–535, https://doi.org/10.1016/j.micpath.2018.08.003.

[45] A. Lingesh, D. Paul, V.G.M. Naidu, N. Satheeshkumar, AMPK activating and anti adipogenic potential of Hibiscus rosa sinensis flower in 3T3-L1 cells, J. Ethnopharmacol. 233 (2019) 123–130, https://doi.org/10.1016/j.jep.2018.12.039.

[46] H.M. Shen, C. Chen, J.Y. Jiang, Y.L. Zheng, W.F. Cai, B. Wang, Z. Ling, L. Tang, Y. H. Wang, G.G. Shi, The N-butyl alcohol extract from Hibiscus rosa-sinensis L. Flowers enhances healing potential on rat excisional wounds, J. Ethnopharmacol. 198 (2017) 291–301, https://doi.org/10.1016/j.jep.2017.01.016.

[47] K.H. Goldberg, A.C. Yin, A. Mupparapu, E.P. Retzbach, G.S. Goldberg, C.F. Yang, Components in aqueous Hibiscus rosa-sinensis flower extract inhibit in vitro melanoma cell growth, J. Tradit. Complement. Med. 7 (2017) 45–49, https://doi.org/10.1016/j.jtcme.2016.01.005.

[48] J. Shunmuga Vellan, P. Lakshmanan, D. Basker Reddy, Formulation development and characterization of Hibiscus rosa-Sinesis dry leaves mucilage as smart polymer for pharmaceutical use, Int. J. Appl. Res. Nat. Prod. 8 (2015) 28–36.

[49] M. Kaleemullah, K. Jiyauddin, E. Thiban, S. Rasha, S. Al-Dhalli, S. Budiasih, O. E. Gamal, A. Fadli, Y. Eddy, Development and evaluation of Ketoprofen sustained release matrix tablet using Hibiscus rosa-sinensis leaves mucilage, Saudi Pharm. J. 25 (2017) 770–779, https://doi.org/10.1016/j.jsps.2016.10.006.

[50] J.Y. Salib, E.N. Daniel, M.S. Hifnawy, S.M. Azzam, I.B. Shaheed, S.M. Abdel-Latif, Polyphenolic compounds from flowers of hibiscus rosa-sinensis linn. And their inhibitory effect on alkaline phosphatase enzyme activity in vitro, Zeitschrift Fur Naturforsch. - Sect. C J. Biosci. 66 (2011) 453–459, https://doi.org/10.1515/znc-2011-9-1003.

[51] M. Ali, P. Alam, V. Singh, M. Jameel, S. Sultana, Phytochemical investigations of the leaves and flowers of Hibiscus rosa-sinensis L, Indian J. Drugs Dermatol. 54 (2017) 30–37.

[52] K.K.T. Goh, L. Matia-Merino, J.H. Chiang, R. Quek, S.J.B. Soh, R.G. Lentle, The physico-chemical properties of chia seed polysaccharide and its microgel dispersion rheology, Carbohydr. Polym. 149 (2016) 297–307, https://doi.org/10.1016/j.carbpol.2016.04.126.

[53] J. Wadhwa, A. Nair, R. Kumria, Potential of plant mucilages in pharmaceuticals and therapy, Curr. Drug Deliv. 10 (2013) 198–207, https://doi.org/10.2174/156720181310020006.

[54] L.M. Pereira, E. Hatanaka, E.F. Martins, F. Oliveira, E.A. Liberti, S.H. Farsky, R. Curi, T.C. Pithon-Curi, Effect of oleic and linoleic acids on the inflammatory phase of wound healing in rats, Cell Biochem. Funct. 26 (2008) 197–204, https://doi.org/10.1002/cbf.1432.

[55] T.K. Lin, L. Zhong, J.L. Santiago, Anti-inflammatory and skin barrier repair effects of topical application of some plant oils, Int. J. Mol. Sci. 19 (2018) 1–21, https://doi.org/10.3390/ijms19010070.

[56] P.H. Lin, M. Sermersheim, H. Li, P.H.U. Lee, S.M. Steinberg, J. Ma, Zinc in wound healing modulation, Nutrients 10 (2018), https://doi.org/10.3390/nu10010016.

[57] O. Chow, A. Barbul, Immunonutrition: Role in Wound Healing and Tissue Regeneration, Adv. Wound Care 3 (2014) 46–53, https://doi.org/10.1089/wound.2012.0415.

[58] R.M. Vignesh, B.R. Nair, Extraction and characterisation of mucilage from the leaves of Hibiscus rosa-Sinensis Linn, Malvaceae), Int. J. Pharm. Sci. Res. 9 (2018) 2883–2890.

[59] J.H. Oh, Y.K. Kim, J.Y. Jung, J. eun Shin, K.H. Kim, K.H. Cho, H.C. Eun, J. H. Chung, Intrinsic aging- and photoaging-dependent level changes of glycosaminoglycans and their correlation with water content in human skin, J. Dermatol. Sci. 62 (2011) 192–201, https://doi.org/10.1016/j.jdermsci.2011.02.007.

[60] P. Sikareepaisan, U. Ruktanonchai, P. Supaphol, Preparation and characterization of asiaticoside-loaded alginate films and their potential for use as effectual wound

dressings, Carbohydr. Polym. 83 (2011) 1457–1469, https://doi.org/10.1016/j.carbpol.2010.09.048.
[61] Q.S. Zhao, Q.X. Ji, K. Xing, X.Y. Li, C.S. Liu, X.G. Chen, Preparation and characteristics of novel porous hydrogel films based on chitosan and glycerophosphate, Carbohydr. Polym. 76 (2009) 410–416, https://doi.org/10.1016/j.carbpol.2008.11.020.
[62] N. Shimizu, M. Tomoda, M. Adachi, Plant mucilages. XXXIX. A representative mucilage, "Hibiscus- mucilage SL, Chem. Pharm. Bull. 34 (1986) 4133–4138, https://doi.org/10.1248/cpb.34.4133.
[63] L. John, L. DiNatale, K. Ertel, J. Leyden, Placebo controlled clinical evaluation of a topical moisturizer formula containing phytol, J. Am. Acad. Dermatol. 76 (2017) AB199, https://doi.org/10.1016/j.jaad.2017.04.776.
[64] M. Abbas, N. Al-Rawi, M. Abbas, I. Al-Khateeb, Naringenin potentiated β-sitosterol healing effect on the scratch wound assay, Res. Pharm. Sci. 14 (2019) 566, https://doi.org/10.4103/1735-5362.272565.
[65] T.S. Lin, A. Abd Latiff, N.A. Abd Hamid, W.Z.B. Wan Ngah, M. Mazlan, Evaluation of topical tocopherol cream on cutaneous wound healing in streptozotocin-induced diabetic rats, Evidence-Based Complement, Altern. Med. 2012 (2012), https://doi.org/10.1155/2012/491027.
[66] X. Chuah, P. Okechukwu, F. Amini, S. Teo, Eicosane, pentadecane and palmitic acid: the effects in in vitro wound healing studies, Asian Pac. J. Trop. Biomed. 8 (2018) 490, https://doi.org/10.4103/2221-1691.244158.
[67] F.A. Ismail, J. Napaporn, J.A. Hughes, G.A. Brazeau, In situ gel formulations for delivery: release and myotoxicity studies, Pharm. Dev. Technol. 5 (2000) 391–397, https://doi.org/10.1081/PDT-100100555.
[68] B.T. Hima, M. Vidyavathi, K. Kavitha, T. Sastry, K.R. Suresh, Preparation and evaluation of ciprofloxacin loaded chitosan-gelatin composite films for wound healing activity, Int. J. Drug Deliv. Technol. 2 (2010) 173–182, https://doi.org/10.5138/ijdd.2010.0975.0215.02027.
[69] Z. Qian, M. Dai, X. Zheng, X. Xu, X. Kong, X. Li, G. Guo, F. Luo, X. Zhao, Y.Q. Wei, Chitosan-alginate sponge: preparation and application in curcumin delivery for dermal wound healing in rat, J. Biomed. Biotechnol. 2009 (2009) 1–8, https://doi.org/10.1155/2009/595126.
[70] V.C. Nguyen, V.B. Nguyen, M. Hsieh, Curcumin-loaded chitosan / gelatin composite sponge for wound healing application, Int. J. Polym. Sci. 2013 (2013).
[71] M.C. Silva, C.T. Andrade, Evaluating conditions for the formation of chitosan/gelatin microparticles, Polimeros 19 (2009) 133–137, https://doi.org/10.1590/S0104-14282009000200010.
[72] U. Bertram, R. Bodmeier, In situ gelling, bioadhesive nasal inserts for extended drug delivery: in vitro characterization of a new nasal dosage form, Eur. J. Pharm. Sci. 27 (2006) 62–71, https://doi.org/10.1016/j.ejps.2005.08.005.
[73] M. Goldberg, A. Manzi, E. Aydin, G. Singh, P. Khoshkenar, A. Birdi, B. LaPorte, A. Krauskopf, G. Powell, J. Chen, R. Langer, Development of a nanoparticle-embedded chitosan sponge for topical and local administration of chemotherapeutic agents, J. Nanotechnol. Eng. Med. 5 (2014) 11, https://doi.org/10.1115/1.4030899, 040905.
[74] C.F. Rodriguez, N. Bruneau, J. Barra, D. Alfonso, E. Doelker, Hydrophilic cellulose derivatives as drug delivery carriers: influence of the substitution type on the properties of compressed matrix tablets, in: handb, Pharm. Control. Release Technol. (2000).
[75] L.D.P. Pereira, M.R.L. Mota, L.A.C. Brizeno, F.C. Nogueira, E.G.M. Ferreira, M. G. Pereira, A.M.S. Assreuy, Modulator effect of a polysaccharide-rich extract from Caesalpinia ferrea stem barks in rat cutaneous wound healing: role of TNF-α, IL-1β, NO, TGF-β, J. Ethnopharmacol. 187 (2016) 213–223, https://doi.org/10.1016/j.jep.2016.04.043.
[76] W. Zhang, M. Bei, Kcnh2 and Kcnj8 interactively regulate skin wound healing and regeneration, Wound Repair Regen. 23 (2015) 797–806, https://doi.org/10.1111/wrr.12347.
[77] B.V. Oliveira, P.G. De Barros Silva, J.D.S. Nojosa, L.A.C. Brizeno, J.M. Ferreira, F. B. Sousa, M.R.L. Mota, A.P.N.N. Alves, Tnf-alpha expression, evaluation of collagen, and TUNEL of matricaria recutita L. Extract and triamcinolone on oral ulcer in diabetic rats, J. Appl. Oral Sci. 24 (2016) 278–290, https://doi.org/10.1590/1678-775720150481.
[78] A. Kastin, Handbook of Biologically Active Peptides, Elsevier Inc., 2013, https://doi.org/10.1016/C2010-0-66490-X.
[79] K.S. Park, D.H. Park, The effect of Korean Red Ginseng on full-thickness skin wound healing in rats, J. Ginseng Res. 43 (2019) 226–235, https://doi.org/10.1016/j.jgr.2017.12.006.
[80] L. Chen, Q. Zheng, Y. Liu, L. Li, X. Chen, L. Wang, L. Wang, Adipose-derived stem cells promote diabetic wound healing via the recruitment and differentiation of endothelial progenitor cells into endothelial cells mediated by the VEGF-PLCγ-ERK pathway, Arch. Biochem. Biophys. 692 (2020) 108531, https://doi.org/10.1016/j.abb.2020.108531.
[81] G. Sererslan, E. Altuğ, T. Kontas, E. Atik, G. Avci, Caffeic acid phenetyl ester accelerates cutaneous wound healing in a rat model and decreases oxidative stress, Clin. Exp. Dermatol. 32 (2007) 709–715, https://doi.org/10.1111/j.1365-2230.2007.02470.x.
[82] J. Li, Y.P. Zhang, R.S. Kirsner, Angiogenesis in wound repair: angiogenic growth factors and the extracellular matrix, Microsc. Res. Tech. 60 (2003) 107–114, https://doi.org/10.1002/jemt.10249.
[83] A.M. Soliman, T.S. Lin, N.A. Ghafar, S. Das, Virgin coconut oil and diabetic wound healing: histopathological and biochemical analysis, Eur. J. Anat. 22 (2018) 135–144 (accessed October 8, 2020), http://eurjanat.com/web/paper.php?id=170402as.
[84] W. Horwitz, Official Methods of Analysis of AOAC International, 17th ed., AOAC International, Gaithersburg Md., 2000.
[85] G. Archana, K. Sabina, S. Babuskin, K. Radhakrishnan, M.A. Fayidh, P. Azhagu Saravana Babu, M. Sivarajan, M. Sukumar, Preparation and characterization of mucilage polysaccharide for biomedical applications, Carbohydr. Polym. 98 (2013) 89–94, https://doi.org/10.1016/j.carbpol.2013.04.062.
[86] L. Hartman, Rapid preparation of fatty acid methyl esters from lipids, LAB.PRACT. 22 (1973) 475–476.
[87] K. Ichihara, Y. Fukubayashi, Preparation of fatty acid methyl esters for gas-liquid chromatography, J. Lipid Res. 51 (2010) 635–640, https://doi.org/10.1194/jlr.D001065.
[88] G.E. Moore, R.E. Gerner, H.A. Franklin, Culture of normal human leukocytes, JAMA J. Am. Med. Assoc. 199 (1967) 519–524, https://doi.org/10.1001/jama.1967.03120080053007.
[89] A. Sharma, C. Marceau, R. Hamaguchi, P.W. Burridge, K. Rajarajan, J.M. Churko, H. Wu, K.I. Sallam, E. Matsa, A.C. Sturzu, Y. Che, A. Ebert, S. Diecke, P. Liang, K. Red-Horse, J.E. Carette, S.M. Wu, J.C. Wu, Human induced pluripotent stem cell-derived cardiomyocytes as an in vitro model for coxsackievirus B3-induced myocarditis and antiviral drug screening platform, Circ. Res. 115 (2014) 556–566, https://doi.org/10.1161/CIRCRESAHA.115.303810.
[90] A. Rohman, A. Nugroho, E. Lukitaningsih, Sudjadi, Application of vibrational spectroscopy in combination with chemometrics techniques for authentication of herbal medicine, Appl. Spectrosc. Rev. 49 (2014) 603–613, https://doi.org/10.1080/05704928.2014.882347.
[91] H.M. El-Laithy, G.S. El-Feky, O.A. Elkady, P.M. Zikry, K.M. Yassin, E.A. Amin, H. Saee, H. Saeed, Multi-drug loaded Chitosan/Gelatin composite sponge for dental application, Int. J. Res. Med. & Appl. Sci. 1 (2015).
[92] A. Petchsomrit, N. Sermkaew, R. Wiwattanapatapee, Alginate-based composite sponges as gastroretentive carriers for curcumin-loaded self-microemulsifying drug delivery systems, Sci. Pharm. 85 (2017), https://doi.org/10.3390/scipharm85010011.
[93] H.A. Hazzah, R.M. Farid, M.M.A. Nasra, M.A. El-Massik, O.Y. Abdallah, Lyophilized sponges loaded with curcumin solid lipid nanoparticles for buccal delivery: development and characterization, Int. J. Pharm. 492 (2015) 248–257, https://doi.org/10.1016/j.ijpharm.2015.06.022.
[94] P.K. Mukherjee, R. Verpoorte, B. Suresh, Evaluation of in-vivo wound healing activity of Hypericum patulum (Family: Hypericaceae) leaf extract on different wound model in rats, J. Ethnopharmacol. 70 (2000) 315–321, https://doi.org/10.1016/S0378-8741(99)00172-5.
[95] J.D. Bancroft, M. Gamble, Theory and Practice of Histological Techniques, Elsevier Health Sciences, 2008 (accessed October 8, 2020), https://books.google.com.eg/books/about/Theory_and_Practice_of_Histological_Tech.html?id=Dhn2KispfdQC&redir_esc=y.
[96] S.V. Hosseini, H. Niknahad, N. Fakhar, A. Rezaianzadeh, D. Mehrabani, The healing effect of mixture of honey, putty, vitriol and olive oil in Pseudomonas aeroginosa infected burns in experimental rat model, Asian J. Anim. Vet. Adv. 6 (2011) 572–579, https://doi.org/10.3923/ajava.2011.572.579.